Characterization Experiments of Secondary Arcs on Solar Arrays: Threshold and Duration

doi: info:doi/10.2514/1.49571

JOURNAL OF SPACECRAFT AND ROCKETS
Vol. 47, No. 6, November–December 2010

Characterization Experiments of Secondary Arcs on Solar Arrays: Threshold and Duration

Hirokazu Masui,* Takayuki Ose,† Tomoki Kitamura,‡ Kazuhiro Toyoda,§ and Mengu Cho¶
Kyushu Institute of Technology, Kitakyushu 804-8550, Japan

DOI: 10.2514/1.49571

An electrostatic discharge test performed on a solar array panel is one of the important tests carried out before spacecraft launch to ensure spacecraft reliability in orbit. In this study, the effects of secondary arcs on the solar array, which can cause catastrophic accidents, are considered. The sustained-arc threshold of multijunction and silicon solar arrays was investigated to establish the design guidelines for ensuring the safety of satellite solar arrays. In this experimental study, the string voltage, string current, gap length, and solar-cell type were selected as test parameters. Gap lengths were 0.5, 0.8, 1.0, and 2.0 mm. For 0.5 and 0.8 mm of gap length, a permanent sustained arc occurred under the condition of 1.5 A of string current for 50, 70, 90, and 110 V of string voltage. Furthermore, temporary sustained-arc duration exponentially increased with increasing string current. Temporary sustained-arc duration longer than 1 ms can serve as a practical alarm for the imminent permanent sustained-arc inception.

Nomenclature

C_{BC}	=	bus capacitance, F
C_{ext}	=	external capacitance, F
C_{1-3}	=	cell capacitance, F
I_{peak}	=	peak value of primary-arc current, A
I_{st}	=	string current, A
T_{dur}	=	duration of temporary sustained arc, s
T_{end}	=	end time of primary arc defined as the time when the current becomes 10% of the peak value, s
T_{start}	=	start time of primary arc defined as the time when the current becomes 10% of the peak value, s
V_{bias}	=	bias voltage, V
V_{st}	=	string voltage; the potential difference between the string across the test gap, V

I. Introduction

AS THE size and the power consumption of satellites increase, to efficiently manage the high power, the operational voltage (bus voltage) of satellites has to be increased. Nowadays, many geosynchronous (GEO) telecommunication satellite employs 100 V bus voltage. Furthermore, it was reported that 50% of accidents on satellites occurred on solar arrays, disrupting the satellite power supply.** In the worst case, an anomaly on a solar array can lead to the total loss of a satellite. Electrostatic discharge (ESD) on a solar array panel could cause such a severe accident. As shown in Fig. 1, the solar cells mounted on a satellite solar panel have a cover glass that serves to reduce the radiation effect of the sun. The cover glass may have a different potential with respect to the satellite body due to its high resistivity. When a satellite encounters a substorm in GEO (i.e., an energetic electron flow), the satellite body may have a negative potential as high as the electron energy. However, the cover-glass surface may have a positive potential with respect to the satellite body because of the secondary and photoelectrons emitted from the surface of the cover glass. Such a charging situation is called an inverted potential gradient.

When the differential voltage developed under the inverted potential gradient exceeds a certain threshold value, a pulse discharge occurs [1]. This discharge is called a primary arc (PA). Although extensive measures were taken to prevent the occurrence of PAs for certain satellites, such as conductive coating of an entire satellite surface including solar array cover glass, it is not practical to extend such a prevention method to a commercial GEO telecommunication satellite. Therefore, most of the commercial satellites are still being launched while accepting risks of PAs. It has been known that a PA may degrade the solar-cell electrical output in a manner similar to radiation effects [2]. PAs occur at a boundary called the triple junction, where a plasma, a conductor, and an insulator (cover glass and adhesive) meet. The triple junctions on solar array panels are mainly interconnections of solar cells and solar-cell edges. During the lengthy duration of satellite operation, the output power of solar array panels degrades due to the occurrence of PAs. This degradation is not instantaneous but cumulative. Therefore, the power-generation capability of these panels should be designed with a sufficient margin by taking into account the power reduction due to radiation and the occurrence of PAs.

A more serious discharge that is induced by a PA can result in instantaneous satellite power loss. It is called a secondary arc or a sustained arc (SA). Since solar cells are placed as densely as possible to reduce the area and mass of the solar panel, adjacent solar-cell strings may have a voltage as high as the bus voltage across a distance (gap length) of 1 mm or less. When a PA occurs at the cell edge facing another string, the gap is filled with dense arc plasma, and the two strings are momentarily short-circuited. As a result, the current generated by the solar array flows into the arc plasma rather than being consumed by the satellite load. The current maintains the arc plasma at a high temperature. In turn, the high-temperature plasma lowers the resistance of the insulator sheet located over the substrate between the two strings and eventually damages the sheet. Generally, the pulse width of PAs is of the order of 100 μs at maximum [3]. On the other hand, the secondary arcs can be sustained for over 1 ms. If a secondary arc exists for a long duration, the insulator sheet is carbonized, and a conductive path is formed between the solar cells and the substrate. Then, the solar array strings and the substrate are

Received 1 March 2010; revision received 6 June 2010; accepted for publication 9 June 2010.

*Postdoctoral Fellow, Department of Electric Engineering, 1-1 Sensui Tobata-ku; masui@ele.kyutech.ac.jp.

†Graduate Student; currently at NEC Toshiba Space Systems, Space Engineering Division.

‡Graduate Student; currently at Mitsubishi Electric Corporation, Space System Department.

§Associate Professor, Laboratories of Spacecraft Environment Engineering, 1-1 Sensui Tobata-ku; toyoda@ele.kyutech.ac.jp. Member AIAA.

¶Professor, Department of Electrical Engineering, 1-1 Sensui Tobata-ku; cho@ele.kyutech.ac.jp. Senior Member AIAA.

**Data located at http://www.lr.tudelft.nl/live/pagina.jsp?id=ed766dad-dc20-44b8-9153-c89014139d0b&lang=en [retrieved 26 April 2010].

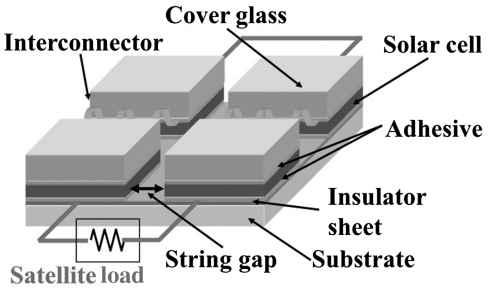

Fig. 1 Schematic of solar array.

permanently short-circuited, leading to permanent power loss. Reference [4] reported that the Tempo-2 satellite suffered a power loss of approximately 10% of its total satellite power. In the case of the Advanced Earth Observing Satellite 2 (ADEOS-2), although the power loss was due to a secondary arc between the power cables, 80% of the satellite power was lost due to a single arc [5].

Secondary arcs are classified into the following three types (see Fig. 2):

1) The first type is non-SA (NSA). The short-circuit current provided by an external power source (i.e., a solar array) flows only while the PA current continues.

2) The second type is temporary SA (TSA). The short-circuit current provided by the external power source lasts longer than a PA current pulse but terminates itself without leaving a permanent conductive path.

3) The third type is permanent SA (PSA). The short-circuit current provided by the external power source keeps flowing until the power source is intentionally shutdown. A permanent SA leaves a permanent conductive path even after the shutdown.

The risk posed by secondary arcs has been recognized by satellite makers and space agencies. The use of a high-bus voltage increases the risk of secondary arcing. Therefore, a reliable design is demanded to suppress the detrimental effects of secondary arcing, as it may directly lead to instantaneous and permanent satellite power loss. Many studies have been performed to understand the physical mechanism of secondary arcing and to determine the threshold of secondary arcing [4,6–13]. In particular, [11] gives the secondary arc threshold of a Si solar cell for various string voltages and currents in a plasma environment. The test circuit of [11] is similar to our circuit, using two power supplies.

Many parameters must be considered in tests conducted for characterizing secondary arcing phenomena. These include types of solar cells, string voltage, string current, and gap between cells. The characteristics of PAs, such as the peak current, pulse width, and arc energy, are also important parameters for analyzing whether the PA makes a transition to a secondary arc. To know the relationship among these parameters, the Japan Aerospace Exploration Agency (JAXA) has promoted an experimental project since 2005. This project is called the Spacecraft Design Guideline Working Group 1 (WG1) [14]. The main purpose of WG1 is to provide design guidelines for preventing spacecraft charging. As a part of the WG1 project, a test to characterize secondary arcing phenomena was conducted at the Kyushu Institute of Technology (KIT) in Japan.

In this paper, we describe the experimental results of the WG1 project. The main purpose of this study is to obtain a table of secondary arc thresholds for a given set of voltages, currents, cell gap lengths, and cell types. This table will give a helpful guidance about how to lay down solar cells on a solar panel to avoid the permanent SA when one considers a future solar-panel design. The statistical data of TSA duration are also presented, and their dependence on each parameter is discussed.

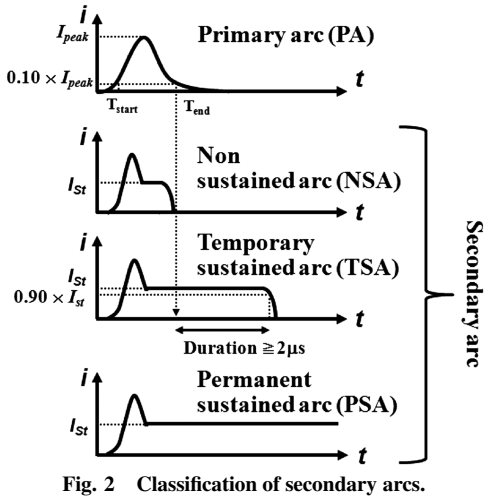

Fig. 2 Classification of secondary arcs.

II. Experimental Setup

A. Test Coupons

Figure 3 shows a photograph of a test coupon. In one coupon, there were three columns (R, B, and G) of four solar-cell strings made of two cells connected in series. For the secondary arc test, nine gaps were available. The solar cell was either a multijunction (MJ) GaAs/InGaP/Ge solar cell or a Si solar cell with gap distances of 0.5, 0.8, 1.0, and 2.0 mm. We used eight coupons in this test. Two coupons each were used for 0.5, 0.8, and 1.0 mm. For 2 mm and Si, one coupon each was available. The quality of solar cells was comparable to that of the ones to be used for a flight model. In the present test, we focused on secondary arcing in the string gaps. Primary discharges at interconnectors could have decreased the test efficiency, hence all interconnectors and bypass diodes were covered with a polyimide tape. In addition, the bus bars were coated with room-temperature vulcanization (RTV).

Figure 4 shows typical microscopic pictures of 0.8 mm gaps. The gap distance is defined by the distance between adjacent solar cells. The gap length varies from point to point. There is about a ±20% variation in the gap length from the design value. In the present paper, we refer to the gap length using the design value provided by the manufacturer. As shown in Fig. 4a, there is no observable feature in the gap. In some regions, as shown in Fig. 4b, the RTV Si adhesive was observed leaking from beneath the solar cells. The leaking of RVT probably occurred during the manufacture of the array while the solar cells were being attached to the polyimide sheet. When RTV leaks, the net gap length becomes shorter than the designed gap length. However, we left the RTV leak as it is, because it represented the operating condition of an actual solar cell.

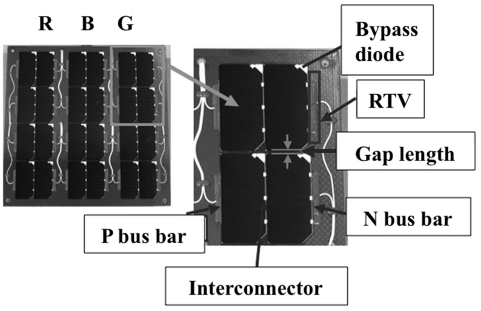

Fig. 3 Photograph of test coupon.

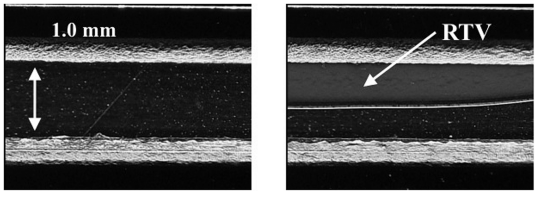

a) Normal gap **b) Leaking of RTV into the gap**

Fig. 4 Pictures of gaps (gap length: 0.8 mm).

B. Experimental Systems

Figure 5 shows a schematic of the measurement system. Experiments were conducted in two vacuum chambers having sizes of 0.6×0.9 m and 1.0×1.2 m. During the experiments, the pressure of each chamber was maintained below about 2.0×10^{-4} Pa. We used an electron beam (reflected high-energy electron diffraction 30 keV, 300 μA) to charge the coupons, which simulates the charging in a GEO. By focusing it, we could control its irradiation area. Furthermore, by concentrating the occurrence positions of PAs near the active gap (i.e., the gap with a voltage applied), the test efficiency was improved greatly. We focused an electron beam to cover the solar-cell area, and its area was 0.01 m^3. The beam energy and the current density were 5 keV and 5–10 mA/m^2, respectively. This electron current density was higher than the actual condition of GEO by about 1000 times. The much higher current density was used to increase the frequency of PAs. In the present test, the electron beam was used only to trigger a PA at the gap. Once a PA occurs, most of the energy is provided by the external capacitance. Therefore, the external circuit and the vacuum environment surrounding the coupon determine the PA waveform. After the PA occurs and an appropriate energy is given to the arc plasma, whether it becomes a secondary arc or not is mostly affected by the available current and voltage, the gap geometry, and material. How the PA was initiated or how the cover glass was charged affected the transition from a PA to a secondary arc very little. The test coupons were mounted on a glass or acrylic plate to isolate them from the chamber. The discharge current (DC) waveforms were acquired by using current probes (DC to 10 MHz and DC to 50 MHz) and were stored in a PC with a data acquisition board (20 MHz). To acquire the waveforms of primary and secondary arcs with different pulse widths, we used two sampling rates, namely, 100 and 20 MHz. For a 100 kHz sampling, the maximum data acquisition duration for a secondary arc was 10 ms. The string voltage V_{st} was measured by an isolation oscilloscope (20 MHz) that

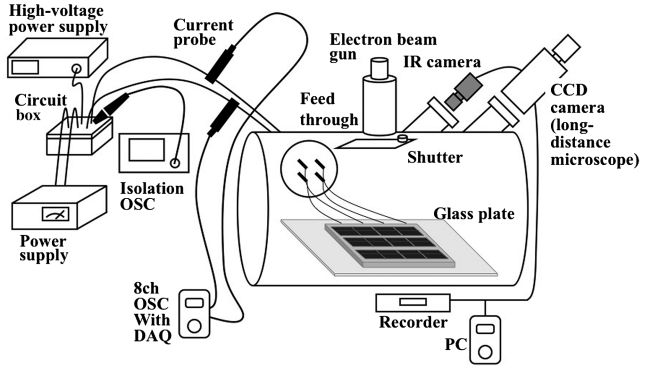

Fig. 5 Schematic of experimental setup. (DAQ: data acquisition, CCD: charge-coupled device, OSC: oscilloscope.)

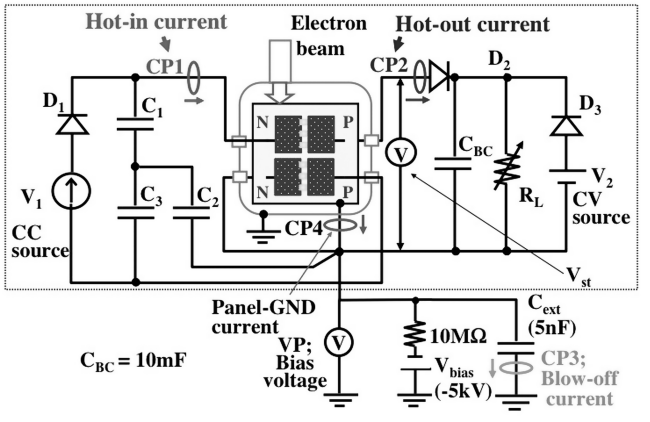

Fig. 6 Test circuit for secondary arc test. CP, CC, CV, VP, and GND represent current probe, constant current, constant voltage, voltage probe, and ground, respectively.

Table 1 Values of C_1, C_2, and C_3.

Cell	Condition	Capacitance, nF C_1	C_2	C_3
MJ	$L_{gap} = 0.5$, 0.8, and 1.0 mm $V_{st} = 30$ to 110 V	27	26	27
MJ	$L_{gap} = 2.0$ mm $V_{st} = 200$ and 300 V	18	100	28
Si	$L_{gap} = 0.5$ mm $V_{st} = 50$ to 110 V	23	420	23

was powered by a battery to isolate the oscilloscope from the bias voltage of −5 kV applied to the coupon and the circuit. Discharge images were captured by an infrared (IR) camera mounted on top of the chamber. In addition, we observed arc spots between gaps in situ by means of a long-distance microscope (Questr QM1, magnification: 70×, focal length: 0.55 to 1.7 m) located outside of the chamber.

C. Experimental Circuit

Figure 6 shows the experimental circuit. The circuit enclosed by the dotted lines simulates a satellite power circuit during power generation. In this circuit, the DC power supply V_1 acts as a constant current source, and V_2 acts as a constant voltage source. For V_1, we used a solar array simulator or a CRD power supply, which was developed at KIT [15]. R_L represents the load resistance. C_1, C_2, and C_3 denote the combined capacitance of solar-cell strings; their values differ, depending on the type of solar cells considered [16], and are listed in Table 1. The top row of Table 1 corresponds to $V_{st} = 30$ to 110 V. The middle row corresponds to $V_{st} = 200$ and 300 V, respectively. The bottom row lists the values used for the Si cell. In Fig. 6, the circuit outside the dotted lines simulates the satellite potential with respect to the ambient plasma. It biases the circuit and power supplies enclosed by the dotted lines to −5 kV. C_{ext} determines the energy of a PA. We set C_{ext} to be 5 nF for all the test cases presented in this paper.

D. Experimental Procedure

There were two stages in the secondary arc test. The first stage was intended to determine the TSA threshold; the second stage was intended to determine the PSA threshold. The test procedure is shown in Fig. 7. In the TSA threshold test, whether a TSA occurred or not within 30 PAs was examined for a fixed set of the string voltage V_{st} and the string current I_{st} in the same test gap. If a TSA did not occur, the string current I_{st} was increased by 0.5 A. This was repeated until we observed a TSA. For one value of the string voltage, we used the same gap. We define the end time of a PA T_{end} as the time when the PA current drops below 10% of the peak value I_{peak} (see Fig. 2). The

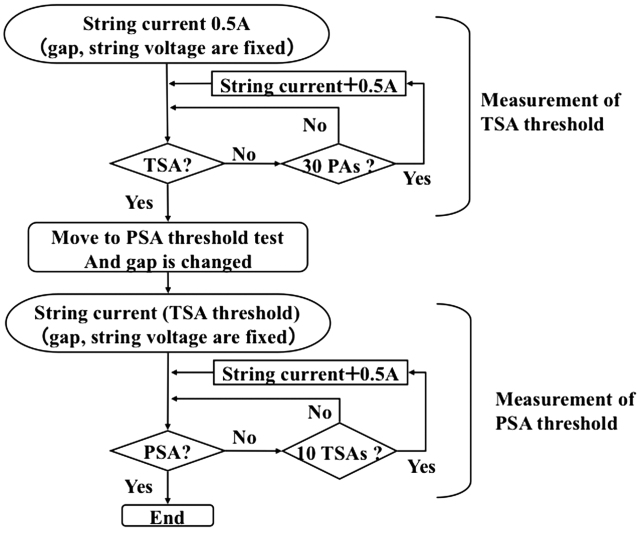

Fig. 7 Scheme of SA threshold test.

duration of the secondary arc T_{dur} is defined from T_{end} to the time when the arc current drops below 90% of the set string current. To judge whether a secondary arc is a TSA or NSA, a secondary arc having T_{dur} over 2 μs is considered a TSA.

Once the TSA threshold was identified, we conducted the PSA threshold test. The PSA threshold test started from the TSA threshold condition. In this test, whether a PSA occurred or not within 10 TSAs was examined for a fixed set of the string voltage V_{st} and the string current I_{st} in the same gap. This procedure was repeated until a PSA occurred. To judge whether an observed arc was a PSA or not, we waited for at least 1 s before we turned off the power supply.

One single pair of two-series connected solar cells was used for the TSA test and another pair was used for the PSA test. The number of TSAs in the PSA threshold test was selected as 10 to ensure the cumulative effect of TSA arc spots if it existed. This cumulative effect is discussed in the Appendix.

III. Experimental Results

A. Sustained-Arc Threshold

This section describes the results of the SA threshold tests discussed in Sec. II.D. Tables 2–5 summarize the TSA and PSA thresholds for the gap lengths of 0.5, 0.8, 1.0, and 2.0 mm for an MJ cell. The string voltage of V_{st} ranged from 30 to 110 V, in steps of 20 V, and the I_{st} increment was 0.5 A. For the 1.0 mm gap and the 110 V V_{st}, the increment in I_{st} was smaller than that for other gap lengths. We also added the test condition of $I_{st} = 4.0$ A for $V_{st} =$ 30 V and gap lengths of 0.8 and 1.0 mm. The following characteristics of secondary arcs were found:

1) No SAs occur for any value of I_{st} with $V_{st} = 30$ V.

2) Under the conditions of low V_{st} and I_{st}, a long gap length suppresses the transition from a PA to a secondary arc.

Table 2 SA thresholds for MJ solar cell with gap length of 0.5 mm

	String voltage, V				
String current, A	30	50	70	90	110
0.5	PA	TSA	TSA	TSA	TSA
1.0	PA	TSA	TSA	TSA	TSA
1.5	PA	PSA	PSA	PSA	TSA
2.0	PA	N/A	N/A	N/A	PSA

Table 3 SA thresholds for MJ solar cell with gap length of 0.8 mm

	String voltage, V				
String current, A	30	50	70	90	110
0.5	PA	PA	TSA	TSA	TSA
1.0	PA	TSA	TSA	TSA	TSA
1.5	PA	TSA	PSA	TSA	PSA
2.0	PA	PSA	N/A	PSA	N/A
4.0	PA	N/A	N/A	N/A	N/A

Table 4 SA thresholds for MJ solar cell with gap length of 1.0 mm

	String voltage, V				
String current, A	30	50	70	90	110
0.5	PA	PA	NSA	TSA	TSA
1.0	PA	PA	TSA	TSA	TSA
1.5	PA	TSA	PSA	PSA	TSA
2.0	PA	PSA	N/A	N/A	PSA
4.0	PA	N/A	N/A	N/A	N/A

Table 5 SA thresholds for MJ solar cell with gap length of 2.0 mm

	String voltage, V				
String current, A	50	70	110	200	300
0.5	PA	TSA	TSA	TSA (+0.2)	TSA (+0.1)
1.0	PA	N/A	TSA	TSA (+0.1)	TSA (+0.1)
1.5	N/A	N/A	TSA	TSA (−0.2)	TSA (−0.2)
2.0	N/A	N/A	PSA	N/A	N/A

3) The PSA threshold strongly depends on I_{st} rather than V_{st}, and a PSA occurs with an I_{st} as low as 1.5 A. Thus, the PSA threshold can be defined as $I_{st} = 1.5$ A.

Even when we increased the string current to 4.0 A for 30 V, no secondary arc was observed. The first characteristic indicates that there is a well-defined threshold for secondary arcs.

The second characteristic is apparent in the results for the gap length of 1.0 mm. The TSA threshold increased with the increasing gap length. There was no TSA for the values of 50 V, 1.0 A or 70 V, 0.5 A, at which TSAs were observed for 0.8 and 0.5 mm.

With regard to the third characteristic, a PSA occurred at $I_{st} = 1.5$ or 2.0 A, even with a string voltage of 50 V. For a string voltage of 110 V, a PSA occurred at $I_{st} = 1.5$ or 2.0 A. The inception of a PSA was independent of the string voltages and the gap lengths within the ranges tested.

We examined the effect of the increasing gap length on secondary arcing by testing the 2.0 mm gap. Higher string voltages of 200 and 300 V were used for the test. Table 5 lists the TSA/PSA thresholds for an MJ solar cell with a gap length of 2.0 mm. It was difficult to maintain the current for the voltages of 200 and 300 V, as we connected CRDs in a series due to their voltage limitation of 100 V. The current fluctuated within ± 0.2 A from the preset value. No SA was observed at the string voltage of 50 V. Although, for a very short duration (maximum 12 μs), a TSA was observed at $V_{st} = 70$ V. A PSA was observed at $V_{st} = 110$ V and $I_{st} = 2.0$ A. For the higher string voltages, such as 200 and 300 V, a SA also occurred. This result shows that extending the gap length is not an effective solution for a high-voltage solar array expected to be used in the near future.

We now discuss the influence of the solar-cell type. A Si solar-cell coupon was tested by following the same procedure as that employed for MJ coupons. The SA threshold of a Si solar cell is listed in Table 6. The TSA threshold voltage was 70 V and was higher than that of an MJ solar cell with the same gap length. A PSA occurred at $I_{st} =$ 1.5 A or more, similar to MJ cells. The reason why the TSA threshold of the Si solar cell was higher than that of the MJ solar cell is probably because the components of the secondary arc plasma were different. When a secondary arc occurs, the arc plasma comprises the ionized gas vaporized from the solar-cell surface. The dominant material for an MJ cell is Ge, for which the melting point is 1211 K, which is less than the melting point of Si of 1687 K. Therefore, arc formation is

Table 6 SA thresholds for Si solar cell with gap length of 0.5 mm

	String voltage, V		
String current, A	50	70	110
0.5	PA	TSA	TSA
1.0	PA	TSA	TSA
1.5	PA	TSA	PSA
2.0	PA	PSA	N/A

Table 7 Characteristic value of PA waveform for $L_{gap} = 0.8$ mm, $V_{st} = 110$ V, and $I_{st} = 1.0$ A

$V_{bias} = -5000$ V	Minimum	Maximum	Average	Standard deviation
Peak current, A	1.72	4.84	3.15	0.99
Charge, μC	22.50	24.54	23.57	0.52
Pulse width, μs	11.40	26.75	17.80	4.77

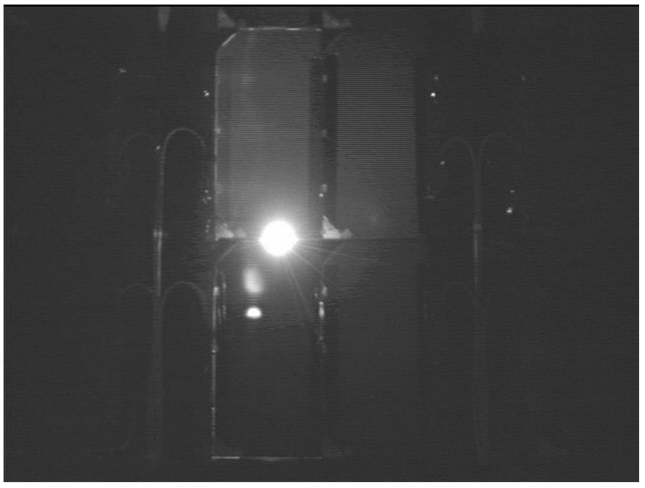

Fig. 8 Typical image of secondary arc.

difficult on a Si solar cell. The results presented in Table 6 agree with those presented in [7,11], except for the difference in the test environments.

The string voltage is the dominant factor for the occurrence of a short-circuit between strings. Once cell strings are short-circuited, the string current is dominant as long as the arc continues. For some gaps, PSA occurred at 1.5 A, while other gaps exhibited PSA at 2.0 A. Because we changed the test gap in the PSA threshold test for each set of V_{st} and I_{st}, the difference may be due to the difference associated with each particular test gap. Although we examined the microscopic images of the PSA location captured before the test, we found no apparent anomaly, such as leaking of RTV or a crack on the polyimide sheet.

B. Typical Discharge Waveform and Image

We now discuss the behavior of the string voltage and current during a secondary arc under the typical conditions of $L_{gap}=$ 0.8 mm, $V_{st} = 110$ V, and $I_{st} = 1.0$ A. Table 7 lists the averaged waveform characteristics of PAs in this condition. The total number of PAs was 14. The averaged value of the pulse width was 17.8 μs in the preceding test case. An example of discharge images is shown in Fig. 8. Figure 9 shows the arc waveforms obtained during the secondary arc shown in Fig. 8. The primary and secondary waveforms are shown at the top, and the voltage waveform is presented at the bottom. The TSA duration of this arc was 510 μs. As soon as the PA occurred, the string current flowed from the hot side to the return side, and the secondary arc current reached the preset value of 1.0 A. After the short-circuit was established, the secondary arc current reached a steady state. On the other hand, the string voltage kept dropping gradually after the end of the PA and was not constant, even at the end of the TSA. In Fig. 10, the TSA waveform of the arc, for which the waveforms are presented in Fig. 9, is shown on a long-time scale; it was acquired with a 100 kHz sampling rate. The secondary arc current was constant, but the string voltage gradually decreased, which implies that the resistance of the secondary arc was changing in time. At the end of the TSA, the lowest string voltage was 29 V. For the other test cases, the lowest string voltage reached during a TSA was approximately 30 V. This value is near the SA threshold listed in Tables 2–4. To induce and sustain a secondary arc, the initial string voltage must exceed 30 V and remain at or above 30 V. Therefore, it is considered that an SA cannot occur if the string voltage of an MJ cell is below 30 V. In the TSA waveforms shown in Figs. 9 and 10, the lowest arc resistance and the maximum power input into the arc plasma were 23Ω and 101 W, respectively.

The test conditions were $L_{gap} = 0.8$ mm, $V_{st} = 110$ V, and $I_{st} = 1.0$ A. The TSA duration was 510 μs. The sampling rate was 20 MS/s.

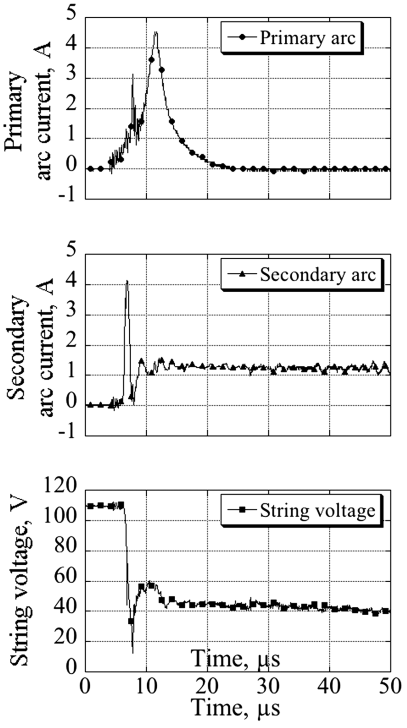

Fig. 9 Typical TSA waveform.

C. Temporary Sustained-Arc Duration

The permanent short-circuit of a solar-cell string gap is caused by a decrease in the resistance of the polyimide sheet due to thermal damage induced by the high-temperature plasma. The thermal damage is proportional to the duration of the short-circuit between strings: that is, TSA duration. TSA duration is an important factor to know the formation of a permanent short-circuit path. In this section, we discuss the statistical data of TSA duration. Table 8 lists the TSA duration data for the gap lengths of 0.5, 0.8, and 1.0 mm. In this table, the number of TSAs and the minimum, maximum, and averaged values of TSA duration are presented. The values with an [a] are beyond the oscilloscope range, and the actual TSA duration is longer than the value listed. TSA duration was not measured in the case of $V_{st} = 70$ V, $I_{st} = 1.5$ and 2.0 A for the gap length of 0.8 mm, because the first SA was a PSA. For the gap lengths of 0.5 and 0.8 mm, the average TSA duration exceeded 1 ms for a current of 1.5 A or higher. For the gap length of 1.0 mm, although some of the averaged TSA durations at 1.5 A were less than 1 ms, they would have been longer than 1 ms if we could measure the long TSAs that lasted for a time exceeding the oscilloscope range of 2 ms.

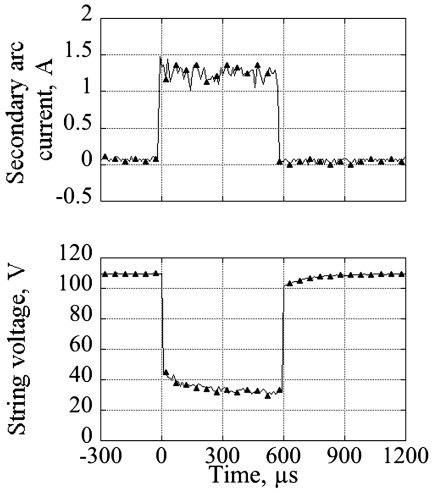

Fig. 10 Typical TSA waveform. The test conditions were $L_{gap} = 0.8$ mm, $V_{st} = 110$ V, and $I_{st} = 1.0$ A. TSA duration was 510 μs.

Table 8 TSA duration for MJ solar cell with gap lengths of 0.5, 0.8, and 1.0 mm

Gap length, mm	String voltage, V	String current, A	Number of TSAs/PAs	TSA duration Min	Max	Ave	Std
0.5	50	0.5	16/133	3	13	7	3
		1.0	14/27	6	66	28	21
		1.5	4/11	2532	6686	4534	1647
	70	0.5	22/55	2	7	4	1
		1.0	11/14	10	1573	250	458
		1.5	2/5	7530	7964[a]	7747	242
	90	0.5	5/34	2	530	54	134
		1.0	10/13	24	650	231	209
		1.5	1/2	7870[a]	7870[a]	7870	——
	110	0.5	10/36	3	9	5	2
		1.0	10/12	3	3180	552	928
		1.5	10/12	13	7840	3176	2558
0.8	50	1.0	22/78	3	730	47	150
		1.5	10/38	6	7126[a]	4086	2797
	70	1.5	14/35	2532	14	7	3
		0.5	9/15	2	688	209	208
	90	1.0	17/27	2	8	4	2
		1.5	17/27	7530	375	41	87
		0.5	11/24	2	7604[a]	4384	2174
	110	1.0	14/20	3	6	3	1
		1.5	14/14	7870[a]	567	179	217
		0.5	3/3	3	7547[a]	7408	197
1.0	50	1.5	9/115	13	1326[a]	983	587
	70	1.5	15/22	3	104	21	25
		1.5	9/14	62	1372[a]	1225	436
	90	0.5	6/30	2	4	3	1
		1.0	7/9	3	14	7	4
		1.5	11/23	7	1372[a]	415	550
	110	0.5	22/30	2	13	5	3
		1.0	10/11	10	78	36	22
		1.2	10/10	14	422	197	164
		1.4	10/10	23	1376[a]	741	536
		1.5	11/11	17	1576[a]	934	579
		1.6	10/10	7	2587[a]	1421	682
		1.8	10/10	64	7840[a]	2793	2533

[a]Values exceed oscilloscope range.

For all the gap lengths, a long TSA duration was observed for large I_{st}. Figure 11 plots the TSA duration for the gap length of 1.0 mm against I_{st}. Each column represents a string current of 0.5, 1.0 and 1.5 A, respectively. The top and bottom bars indicated with each data point correspond to the maximum and the minimum values, respectively. It is observed that TSA duration exponentially increases with increasing I_{st}. Although there are slight differences among the string voltages for 0.5 and 1.0 A, the order of magnitude of the TSA durations is the same for the different string voltages. It is evident that TSA duration strongly depends on the string current. In Sec. III.A, PSA threshold was defined as a string current of 1.5 A or higher.

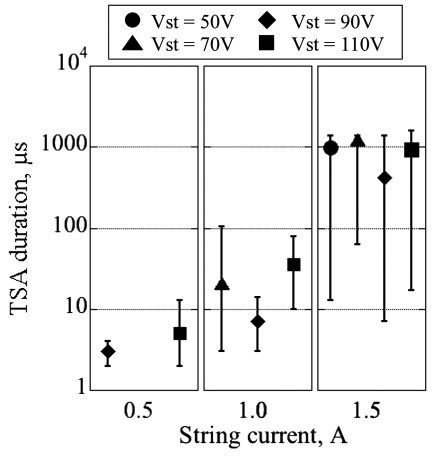

Fig. 11 TSA duration for MJ solar cell with gap length of 1.0 mm.

Table 9 TSA duration for MJ solar cell with gap length of 2.0 mm

String voltage, V	String current, A	Number TSAs/PAs	TSA duration Min	Max	Ave	Std
70	0.5	5/48	2	12	6	5
110	0.5	4/30	2	3	2	0
	1.0	30/36	4	2270	144	502
	1.5	11/23	785	3007	1408	608
	2.0	5/23	531	5370[a]	3917	1990
200	0.7	22/55	2	20	7	5
	1.1	11/14	3	1080	108	283
	1.3	2/5	5	221	60	77
300	0.6	6/64	2	3	2	0
	1.0	10/13	6	163	63	61
	1.3	13/14	7	1040	372	97

[a]Values exceed oscilloscope range.

Table 10 TSA duration for Si solar cell with gap length of 0.5 mm

String voltage, V	String current, A	Number TSAs/PAs	TSA duration Min	Max	Ave	Std
70	0.5	10/31	2	5	3	1
	1.0	12/16	6	482	88	133
	1.5	10/18	5	1595	1098	385
110	0.5	10/26	3	8	4	1
	1.0	9/18	4	590	233	216
	1.5	6/11	18	1972	727	727

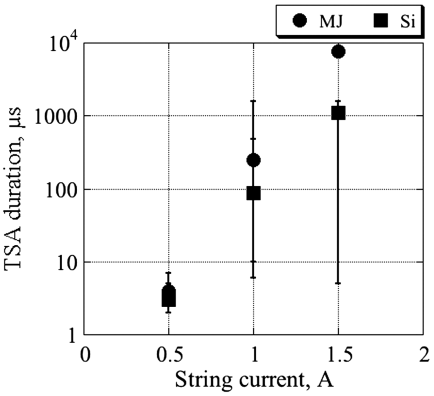

Fig. 12 TSA duration for MJ and Si solar cells for 70 V and 0.5 mm gap length.

From Fig. 11, TSA duration is estimated to be over 1 ms for 1.5 A. It is a matter of time for a TSA to become a PSA once a TSA longer than 1 ms is observed.

Table 9 lists the TSA duration for the gap length of 2.0 mm. A PSA occurred at $V_{st} = 110$ V and $I_{st} = 2.0$ A, and the TSA duration again exceeded 1 ms. Even though the gap length is extended, the TSA duration of 1 ms is still a good indicator as an alarm against PSA transition. For high-string voltages of 200 and 300 V, TSA durations longer than 1 ms were also observed. Even if we extend the gap length, once a short-circuit occurs across a gap, the short-circuit duration strongly depends on the string current, which is a trend similar to that observed in the cases of short gaps.

Table 10 lists the statistical data of TSA duration for a Si solar cell. The string current was again a dominant factor in increasing the TSA duration. Figure 12 shows a comparison of TSA durations for MJ and Si solar cells. For the test condition with equal V_{st} and I_{st}, TSA duration for the Si solar cell was shorter than that for the MJ solar cell, even after adding the standard deviation to the average values. This is probably because of the difference between the solar-cell materials.

In the early phase of a secondary arc, the resistance of the arc plasma in the gap is relatively high, because the plasma temperature is still low. As the arc plasma temperature gradually increases due to joule heating, the arc resistance decreases. Once the arc resistance becomes sufficiently low, the current can easily flow into the arc plasma and maintain the secondary arc. This is a feedback mechanism. The more the current flows, the more stably the arc plasma is maintained. This explains why the string voltage gradually decreases during a TSA and why TSA duration exponentially increases with the current.

IV. Conclusions

In the present paper, we have presented the experimental results that characterize the threshold for secondary arcs on a solar panel. Test coupons made of MJ or Si solar cells were placed in a vacuum chamber and charged using an electron beam to create PAs in the active gap across which a voltage was applied. The gap length, string voltage, string current, and type of a solar cell were selected as the test parameters, and the rating sheet of a NSA, a TSA, and a PSA were defined as a design guideline for a satellite solar panel. No secondary arc was observed for a gap voltage of 30 V for an MJ solar cell and 50 V for a Si solar cell. Once a PA became a TSA, the resistance of the arc plasma decreased gradually with time as the arc current heated the arc plasma. The minimum voltage attained by the voltage across the arc plasma was approximately 30 V, corresponding to the threshold voltage of secondary arc inception. A PSA was observed at a string current of as low as 1.5 A. TSA duration exceeding 1 ms was a good indicator to raise alarm about the risk of the imminent PSA inception. The TSA duration had an exponential dependence on the string current. Extending the gap length to 2 mm was effective in suppressing the secondary arc inception up to 50 V for an MJ solar cell. However, the advantage of the long gap length diminished at a voltage of 70 V or higher.

There was a difference in the threshold values for different types of solar cells. Since the composition of arc plasma varies with the solar-cell material, it affected the arc plasma resistance and consequently led to different thresholds. Thus, to explain this difference regarding the composition of arc plasma, a spectroscopy experiment needs to be performed, such as in [17].

In this paper, we presented the results of secondary arc tests carried out using a fixed amount of PA energy: that is, a fixed set of external capacitance and coupon bias voltage. Whether the characteristics of a PA affect the threshold of secondary arcs or not is a subject of ongoing debate among the worldwide experts. The experiments designed to study the effects of PAs will be presented in another paper.

A. Appendix: Cumulative Effect

We explained the test procedure in Sec. III. Once a TSA occurs in a gap, the metal vapor leaves a conductive arc spot. If many TSAs are concentrated on a particular point in the active gap, the superimposed arc spots may extend the conductive path, practically narrowing the gap length. Eventually, the cumulative TSAs may lead to the permanent short-circuit of the gap (i.e., a PSA). In the present study, because we used the same gap for one set of voltage and current until a PSA was observed, a significant number of TSAs could occur before a PSA occurred. We verified that the cumulative effect of TSAs does not affect the PSA threshold. We used a long-distance microscope placed outside the chamber after each test case of the PSA threshold test. By using the long-distance microscope, no vacuum break was necessary to do the visual inspection. We discussed the results for the 0.5 mm gap length. Figure A1a shows a microscope picture of the gap after the PSA threshold test with $V_{st} = 70$ V and $I_{st} = 1.0$ A. No PSA occurred before this picture was taken, but 33 TSAs occurred with a maximum duration of 1.5 ms. A PSA occurred after two additional TSAs that occurred after we increased the current to 1.5 A. Figure A1b shows the picture taken after a PSA occurred. In Fig. A1a, no arc spots preexisted in the gap, and a PSA occurred in the undamaged region. The cumulative extension of the arc spots, which may form a conductive short-circuit path in the gaps, was not observed.

In addition, for the test case of the gap length of 1.0 mm at 110 V, we gradually increased the string current, as listed in Table 7. Approximately 80 TSAs occurred in the gap before a PSA occurred at $I_{st} = 2.0$ A. Even such a large number of cumulative TSAs did not cause a PSA. Furthermore, the number of PAs at a particular gap or a particular arc spot in an orbit is expected to be much less than 10, considering the large number of solar cells on a real satellite solar panel. Therefore, even if a cumulative effect of TSAs exists, we can practically neglect it.

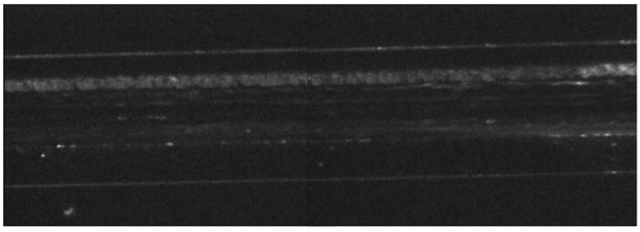

a) Before PSA (V_{st} = 70 V, I_{st} =1.0A)

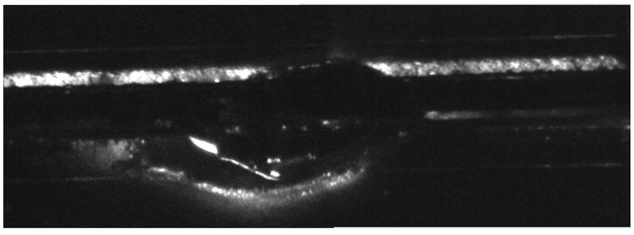

b) After PSA (V_{st} = 70 V, I_{st} = 1.5A)

Fig. A1 Photo taken by using long-distance microscope.

References

[1] Hastings, D., and Garrett, H., *Spacecraft Environment Interactions*, Cambridge Univ. Press, New York, 1996, pp. 142–198.

[2] Okumura, T., Masui, H., Toyoda, K., Imaizumi, M., and Cho, M., "Degradation of Electric Performance due to Electrostatic Discharge on Silicon Solar Cell for Space," *Journal of the Japan Society for Aeronautical and Space Sciences*, Vol. 55, No. 647, 2007, pp. 590–596. doi:10.2322/jjsass.55.590

[3] Amorim, E., Payan, D., Reulet, R., and Sarrail, D., "Electrostatic Discharges on a 1 m^2 Solar Array Coupon Influence of the Energy Stored on Coverglass on Flashover Current," *9th Spacecraft Charging Technology Conference*, Japan Aerospace Exploration Agency (JAXA), Tsukuba, Japan, 2005, pp. 331–344.

[4] Katz, I., Davis, V. A., and Snyder, D. B., "Mechanism for Spacecraft Charging Initiated Destruction of Solar Arrays in GEO," 36th Aerospace Science Meeting, AIAA Paper 98-1002, 1998.

[5] Hosoda, S., Kim, J., Cho, M., Toyoda, K., Kawakita, S., Kusawake, M., Takahashi., M., and Maejima, H., "Ground Investigation of Sustained Arc Phenomena in Power Cables on ADEOS-2 Satellite," *Journal of the Japan Society for Aeronautical and Space Sciences*, Vol. 54, No. 633, 2006, pp. 427–433. doi:10.2322/jjsass.54.427

[6] Snyder, D. B., Ferguson, D. C., Vayner, B. V., and Galofaro, J. T., "New Spacecraft-Charging Solar Array Failure Mechanism," *Proceedings of the 6th Spacecraft Charging Technology Conference*, U.S. Air Force Research Laboratory, Bedford, MA, 1998, pp. 297–301.

[7] Hoeber, C. F., Robertson, E. A., Katz, I., Davis, V. A., and Snyder, D. B., "Solar Array Augmented Electrostatic Discharge in GEO," 17th International Communications Satellite Systems Conference, AIAA Paper 1998-1401, Feb. 1998.

[8] Cho, M., Ramasamy, R., Matsumoto, T., Toyoda, K., Nozaki, Y., and Takahashi, M., "Laboratory Tests on 110-Volt Solar Arrays in Simulated Geosynchronous Orbit Environment," *Journal of Spacecraft and Rockets*, Vol. 40, No. 2, 2003, pp. 211–220. doi:10.2514/2.3955

[9] Cho, M., Kim, J.-H., Hosoda, S., Nozaki, Y., Miura, T., and Iwata, T., "Electrostatic Discharge Ground Test of a Polar Orbit Satellite Solar Panel," *IEEE Transactions on Plasma Science*, Vol. 34, No. 5, 2006, pp. 2011–2030. doi:10.1109/TPS.2006.881935

[10] Gaillot, L., Fille, M.-L., and Levy, L., "Secondary Arcs on Solar Array: Test Results of EMAGS 2," *9th Spacecraft Charging Technology Conference*, Japan Aerospace Exploration Agency (JAXA) , Tsukuba, Japan, 2005, pp. 345–352.

[11] Berthou, C., Boulanger, B., and Levy, L., "Plasma ESD Qualification Test Procedure of Alcatel Alenia Space Solar Array," *IEEE Transactions on Plasma Science*, Vol. 34, No. 5, 2006, pp. 2004–2010. doi:10.1109/TPS.2006.883371

[12] Cho, M., and Goka, T., "Japanese Practices of Solar Array ESD Ground Tests," *9th Spacecraft Charging Technology Conference*, Japan Aerospace Exploration Agency (JAXA), Tsukuba, Japan, 2005, pp. 377–396.

[13] Vayer, B., Ferguson, D., and Galofaro, J., "Detrimental Effect of Arcing on Solar Array Surfaces," *10th Spacecraft Charging Technology Conference* [CD-ROM], Centre National d'Etudes Spatiales, Toulouse, France, June 2007.

[14] Nitta, K., "Spacecraft Design Guideline in JAXA," *Proceedings of the 4th Spacecraft Environment Symposium*, Japan Aerospace Exploration Agency (JAXA), Tsukuba, Japan,2008, pp. 40–49.

[15] Toyoda, K., Aso, S., Kyoku, T., Kitamura, T., and Cho, M., "Proposal of a Current Regulative Diode for Power Supply in Sustained Arc Test," *IEEE Transactions on Plasma Science*, Vol. 34, No. 5, 2006, pp. 1967–1972. doi:10.1109/TPS.2006.881933

[16] Payan, D., Schwander, D., and Catani, J. P., "Risks of Low Voltage Arcs Sustained by the Photovoltaic Power of a Satellite Solar Array during an Electrostatic Discharge Solar Arrays Dynamic Simulator," *Proceedings of the 7th International Spacecraft Charging Technology Conference*, ESA, Noordwijk, the Netherlands, 2001, pp. 447–453.

[17] Vayner, B., Ferguson, D. C., and Galofaro, T., "Emission Spectra of Arc Plasmas," *IEEE Transactions on Plasma Science*, Vol. 36, No. 5, 2008, pp. 2219–2227. doi:10.1109/TPS.2008.2001424

I. Boyd
Associate Editor